


MONITORING LAND COVER DYNAMICS AND FOREST DEGRADATION IN SOUTH SUMATRA PEATLANDS FROM 2015 TO 2023 BY REMOTE SENSING APPLICATION

M. Y. N. Khakim^{*,1} , A. A. Bama¹ , and T. Tsuji² 

¹ Physics Department, Faculty of Mathematics and Natural Sciences, Universitas Sriwijaya, Indonesia

² School of Engineering, University of Tokyo, Japan

* **Correspondence to:** Mokhamad Yusup Nur Khakim, myusup_nkh@mipa.unsri.ac.id

Abstract: Most Peat Hydrological Units (PHU) in South Sumatra, Indonesia, have been threatened by degradation from climate changes, human activities, and environmental factors. This study mapped land cover using Random Forest Classification and identified forest degradation using NDFI (Normalized Difference Forest Index) change analysis in several PHUs of the South Sumatra peatland from 2015 to 2023. We combined Sentinel-1, Sentinel-2, and Landsat-8 data for the land cover classification. Meanwhile, we utilized Landsat-8 to identify forest degradation. Our findings indicate that tree cover significantly decreased in 2015, 2019, and 2023, coinciding with severe drought conditions driven by El Niño events. A significant decrease in forest cover in 2019 was suggested by low tree cover, up to 47.1% of the total area of 1.054 million ha. Therefore, grassland and bare/sparse vegetation had more significant coverage percentages, reaching 22.89% and 11.40%, respectively, in 2019. Deforestation varied but generally decreased from 2015 to 2023, according to the analysis of NDFI changes. Vegetation regrowth increased notably from 2016 to 2020 and remained relatively stable afterward. In addition, forest disturbance decreased from 2015 to 2020 but slightly increased in the last few years. Although two PHUs have encountered more severe degradation, their peatland ecosystems included inside them have distinct characteristics. Specifically, the PHU of Sungai Saleh – Sungai Sugihan encompasses cultivated areas, whereas the PHU of Sungai Sugihan – Sungai Lumpur comprises protected areas. These findings highlight the need for restoration and sustainable land management to prevent further degradation.

Keywords: Peatland, Land cover, Degradation, Random Forest, NDFI, South Sumatra, Remote Sensing.

Citation: Khakim, M. Y. N., A. A. Bama, and T. Tsuji (2024), Monitoring Land Cover Dynamics and Forest Degradation in South Sumatra Peatlands from 2015 to 2023 by Remote Sensing Application, *Russian Journal of Earth Sciences*, 24, ES4012, EDN: YGBEBU, <https://doi.org/10.2205/2024es000914>

RESEARCH ARTICLE

Received: 3 February 2024

Accepted: 28 May 2024

Published: 16 December 2024



Copyright: © 2024. The Authors. This article is an open access article distributed under the terms and conditions of the Creative Commons Attribution (CC BY) license (<https://creativecommons.org/licenses/by/4.0/>).

1. Introduction

Hydrologically and ecologically different peat forest habitats regulate the global carbon cycle, biodiversity, and climate [Page et al., 2011]. Peat forest degradation and land cover changes due to drainage, deforestation, and land conversion pose unprecedented risks to these vital ecosystems [Hooijer et al., 2010; Vijay et al., 2016]. Peatlands are carbon sinks that help mitigate climate change [Page et al., 2011]. Due to soil oxidation and degradation, peat forests emit greenhouse gases when drained and deforested [Hooijer et al., 2010; Khakim et al., 2020].

There are direct and indirect drivers of peatland deforestation and degradation in the study area. Logging, industrial plantations, artificial drainage canals, recurrent fires, and fire-based traditional farming practices are direct contributors. Indirect factors include climate change, land use policy inconsistency, and inadequate management [Dohong et al., 2017]. The logging and industrial plantations driving the degradation by agricultural conversion are mainly for palm oil and acacia plantations [Astuti, 2021; Cooper et al., 2020;

[Miettinen et al., 2012](#); [Nurhayati et al., 2021](#)]. Industrial plantations and small holder areas occupy a minimum of 21% of the peatland in South Sumatra [[Putra et al., 2019](#)]. In addition, the usage of uncontrolled fire has progressively increased over time in relation to the traditional cultivation of sonor or swamp rice [[Chokkalingam et al., 2006](#)]. Land clearance removes woody and non-woody plants for agricultural or industrial use. Logging roads make interior forests simpler to access and move, worsening deforestation. Artificial drainage systems lower the groundwater table for crop cultivation and timber transport. However, drainage systems disrupt the hydrological equilibrium, increasing surface runoff and decreasing water storage capacity. Consequently, the draining of peatlands can alter hydrology and ecosystem processes.

Furthermore, drainage for agricultural and plantation development increases peat soil subsidence and fire risk [[Khakim et al., 2020](#)]. The subsidence rate of peatlands in South Sumatra increased by 6.4 times after the 2015 El Niño event [[Khakim et al., 2020](#)]. In addition, the rate ranged from -567 to 347 mm/year between 2019 and 2022 [[Zheng et al., 2023](#)]. Higher temperatures, less precipitation, and more peat evaporation in droughts reduce peatland groundwater tables. Drawdown accelerates peat oxidation and breakdown, causing subsidence and carbon emissions. Peat fires are a significant issue in Indonesia, notably in South Sumatra. Dry drainage makes peatlands more combustible [[Khakim et al., 2022](#)]. Air pollution and climate change can result from peat fires releasing substantial volumes of carbon dioxide and other pollutants [[Cobb et al., 2017](#); [Dommain et al., 2014](#); [Page et al., 2011](#)].

Sustainable management and peatland degradation have been addressed. Strategies include avoiding peatland conversion, encouraging rewetting and regenerating degraded peatlands, and restricting burning [[Dohong, 2017](#); [Harrison et al., 2019](#); [Uda et al., 2020](#); [Yuwati et al., 2021](#)]. Due to their environmental and climate implications, peatland conservation and management in Indonesia, including South Sumatra, have garnered international attention. Initiatives like the Indonesian Peatland Restoration Agency (BRG) have been established to coordinate restoration efforts [[Humas, 2016](#)]. Information on peatland degradation is essential for designing effective policies and regulations that promote sustainable land use practices, prevent further degradation, and support restoration efforts. Understanding and addressing peatland degradation in South Sumatra is crucial for mitigating climate change, preserving biodiversity, regulating water resources, preventing fires, promoting sustainable agriculture, supporting local communities, meeting international commitments, and maintaining the ecosystem's overall health. The urgent need to understand the drivers and consequences of such changes underscores the importance of advanced remote sensing technologies, which offer invaluable insights for effective conservation strategies [[Miettinen et al., 2017](#)].

Ecological, hydrological, and environmental indices are used to estimate peatland deterioration. Peatland degradation is quantified and monitored in several ways. Satellite imaging (Landsat, Sentinel) can track land cover, vegetation health, and water levels. Using Landsat-8, Sentinel-1, and Sentinel-2 satellite data to analyze peat forest degradation and land cover changes is challenging. Landsat-8's multispectral capabilities allow it to identify deforested areas, agricultural growth, and vegetation health changes [[Pettorelli et al., 2014](#)]. Sentinel-1 SAR technology provides all-weather imaging and reliable water table monitoring, which is crucial for peatland health assessment [[Asmuß et al., 2019](#); [Khakim et al., 2022](#); [Toca et al., 2023](#)]. The spectral richness and high geographical resolution of Sentinel-2 data improve peat forest ecosystem study. Its regular return intervals allow monitoring of land cover changes, revealing subtle changes in vegetation composition and structure [[Carrasco et al., 2019](#); [Poortinga et al., 2019](#); [Urban et al., 2018](#)]. Advanced analytical methods are needed to obtain comprehensive information from these databases.

Unsupervised and supervised classification analyze land cover. Automatic, data-driven unsupervised classification is ideal for land cover pattern research, especially in areas with little prior knowledge. However, unsupervised classification has lower accuracy and subjectivity in interpretation. In addition, unsupervised methods can produce

numerous classes that might not have precise ecological or practical meanings, making interpretation difficult. On the contrary, supervised classification allows us to differentiate between them accurately based on your training samples. On the other hand, random forest classification enables the automated identification and classification of land cover types based on the spectral signatures of different land features, contributing to precise mapping and monitoring [Gómez *et al.*, 2016; Malinowski *et al.*, 2020; Shih *et al.*, 2021; Tian *et al.*, 2016]. It allows for identifying and monitoring degradation-related changes in land cover proportions. Landsat endmembers were successfully applied to derive a Normalized Difference Fraction Index (NDFI) for monitoring forest degradation in several environmental, such as Amazon forest [Souza Jr. *et al.*, 2013], non-Amazonian tropical forest [Schultz *et al.*, 2016], and tropical peatland [Numata *et al.*, 2022]

Spectral analysis examines peatland surface reflectance in different bands. Spectral signatures can reveal vegetation, water, and soil changes. Changes in vegetation composition, density, and health indicate peatland degradation. Monitoring monoculture plantations vs. diversified native vegetation can indicate a decline. Land cover changes caused by peatland forest degradation can have serious ecological, environmental, and socioeconomic consequences. Spectral Mixture Analysis (SMA) is a typical remote sensing approach for assessing land cover component proportions in mixed pixels. Assessing peatland deterioration is another use for it. SMA and machine learning algorithms like random forest classification are used for classifying complicated ecosystems like peat forests. SMA uses remote sensing data to assess the fractional cover of vegetation, soil, and water [Adams, 1995; Sakti and Tsuyuki, 2015].

This study employed a supervised random forest (RF) classification method to gain insight into the various types and spatial distribution of land cover. Furthermore, the SMA and NDFI were utilized to identify peatland vegetation degradation in the South Sumatra peatland. The relationship between peatland forest degradation and land cover refers to how changes in the condition and quality of peatland ecosystems affect the types and distribution of vegetation and other land cover components within those ecosystems.

2. Materials and Methods

2.1. Study area

The study area is peatland, situated on the eastern coast of the island of Sumatra, adjacent to the Musi River delta (Figure 1). The study area is in two Bayuasin and Ogan Ilir Regencies and consists of nine peat hydrological units (PHUs). In 2015, the South Sumatra region experienced a catastrophic event when the El Niño phenomenon triggered devastating fires in its vulnerable peatlands. These fires ravaged a substantial area, estimated to be between 117,367 and 144,410 hectares (ha) of peatland within the province [KLHK, 2020]. The impact of these fires was particularly severe in specific areas, with approximately 6580 ha of burned peatlands located in villages situated within or adjacent to former restoration and conservation project areas in the Banyuasin, Muba, and Ogan Komering Ilir Regencies. Furthermore, an additional 13,061 ha of peatland succumbed to the flames within oil palm plantations, while a staggering 67,846 ha were engulfed in fires within logging concessions [Budiman *et al.*, 2021].

Within the PHU Sugihan-Lumpur area, four villages have implemented livelihood revitalization initiatives and participated in the Peat Care Village programs. These efforts included providing essential livelihood support to the local community. However, it's noteworthy that these villages did not undertake additional restoration activities, such as peat rewetting. Unfortunately, the reliance solely on livelihood revitalization and the programs proved insufficient to mitigate peatland fire risk. From September to October 2019, these villages experienced fires that ravaged 14,113 ha of peatland. A notable fire vulnerability persists despite groundwater monitoring stations in 8 out of 10 restoration areas [Budiman *et al.*, 2021].

While notable progress has been made in peatland protection, significant threats still loom. Before recent conservation endeavors, numerous companies obtained concession

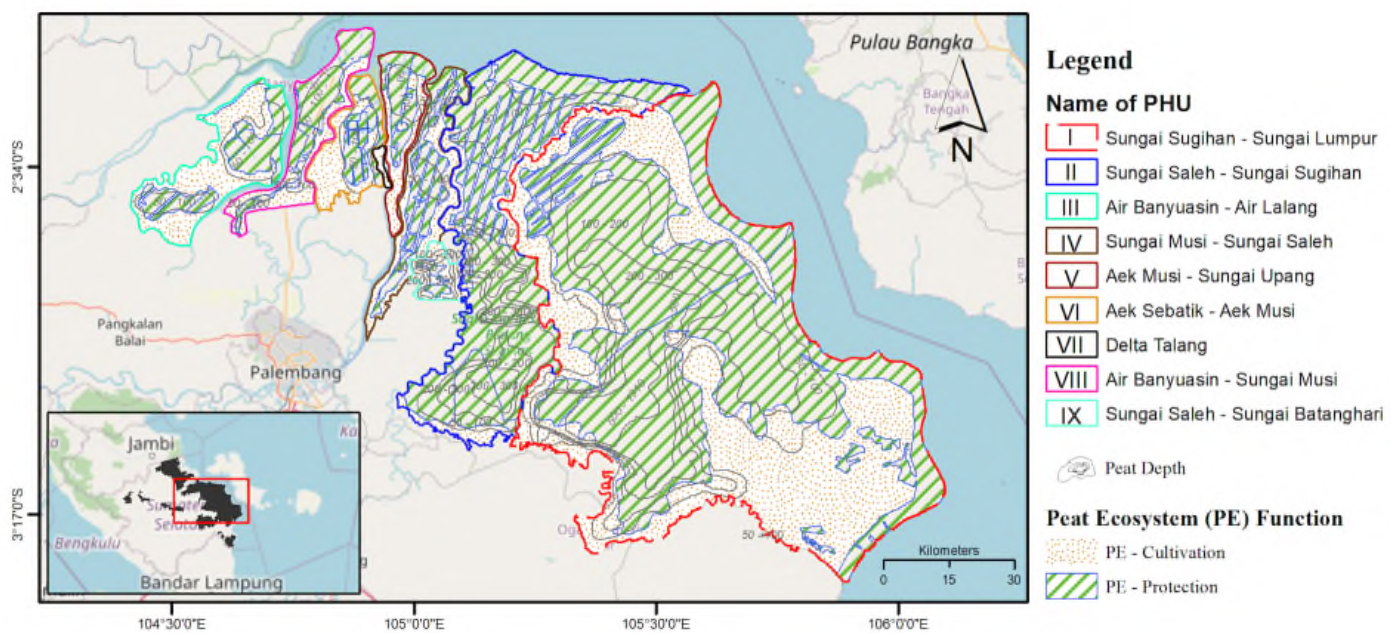


Figure 1. Study area consisting of nine peat hydrological units.

permits encompassing vast protected peatland expanses. Alarming, over 25 percent of the total 12.2 million hectares (30 million acres) of protected peatland has already been allocated for concession areas, primarily geared toward pulpwood and palm oil plantations, or possesses the potential for conversion into plantation or agricultural usage [Hidayah *et al.*, 2018]. It highlights the persistent challenge of safeguarding these critical ecosystems against existing and potential land use pressures.

2.2. Land Cover Classification

We classified land cover over the study area by combining 544 radar images from Sentinel-1 and 2923 optical imageries, comprising 2318 Sentinel-2, and 605 Landsat-8 from January 2015 to August 2023. We preprocessed the image using Google Earth Engine (GEE). The radar data analysis involved using dual-polarized C-band data acquired by the Synthetic Aperture Radar (SAR) instrument aboard the S1A satellite.

The Level-1 Ground Range Detected product (GRD), as provided by GEE, was employed in this analysis. These GRD images underwent radiometric calibration and orthorectification. Two distinct polarization modes were used: single and dual-band co-polarization with vertical transmit/receive (VV) and horizontal receive (VH). An additional preprocessing step was implemented, which involved spatial filtering through a 7×7 Refined Lee speckle filter to mitigate the inherent speckle noise found in radar images. This preprocessing step was crucial for enhancing the suitability of the images for land cover detection at the spatial resolution employed in this research.

Furthermore, additional bands, such as the VH/VV ratio, the normalized ratio procedure between bands (NRPB) [Filgueiras *et al.*, 2019], and the radar vegetation index (RVI) [Yamada, 2015] were generated. For each observation date, a composite image comprising five bands (VV, VH, VH/VV ratio, NRPB, and RVI) was created, as this combination has been identified as optimal for characterizing land cover. Images were temporally combined by calculating median values for each band, resulting in the generation of composites spanning a one-year timeframe.

Sentinel-2 data, processed at level 1C as sourced from GEE, were employed. These data have undergone orthorectification and radiometric correction, resulting in top-of-atmosphere reflectance values. Bands 2 to 8 were selected and four indexes, namely Normalized Difference Vegetation Index (NDVI), Normalized Difference Built-up Index

Table 1. Bands and indices of each satellite for classification

| Satellite | Bands/Indices |
|------------|--|
| Sentinel-1 | VV, VH, VH/VV, NRPB, and RVI |
| Sentinel-2 | B2-8, 11, 12, NDVI, NDBI, S2REP, and IRECI, |
| Landsat-8 | B2-7, soil, GV, NPV, GV _s , shade, and NDFI |

(NDBI), Sentinel-2 Red-Edge Position (S2REP), and Inverted Red-Edge Chlorophyll Index (IRECI), were derived for use, with their initial spatial resolutions at 10 meters. An automated cloud masking procedure was implemented to ensure data quality, utilizing band QA60 from the S2 1C product, effectively masking both opaque and cirrus clouds. Moreover, parameters derived from Landsat-8 are described in the following sub-section.

Table 1 shows the bands of each satellite for the classification input dataset. Several indices were also derived from each dataset to be included as the input. These bands and indices from Sentinel-1, Sentinel-2, and Landsat-8 images were merged into a single fused image using the ‘addBands()’ function in Google Earth Engine. Parameters were derived from unmixed fractions of the Landsat-8, such as Soil, Green Vegetation (GV), Non-Photosynthetic Vegetation (NPV), Shade-normalized Green Vegetation (GV_s), Shade, and NDFI. More relevant feature variables boost classification accuracy [Amoakoh *et al.*, 2021].

Following the standardization of band values through band normalization, band stacking was carried out by aggregating all the processed radar and optical images for input each year. In this study, the Random Forest algorithm has been selected as the classifier. This algorithm assigns equal weight to each of the band layer stack images. Equal weighting in Random Forest (RF) classification ensures all features contribute equally to the model's decision-making process. This approach simplifies the modeling process, prevents bias, makes the model more robust to changes in the dataset, promotes balanced decision-making, and assumes equal importance. The RF approach employs a collection of decision trees to enhance prediction accuracy [Breiman, 2001]. We applied the Random Forest classification algorithm due to its robustness and ability to handle complex land cover patterns.

Based on field observation and image identification, we created point features for different land cover classes. Each point was assigned a class label representing the land cover class. To avoid overfitting, the labeled data was split into training and validation sets, 60% and 40%, respectively. The RF classifier with 120 trees was trained using the training dataset, and the classifier learned the underlying patterns and relationships between the features and class labels in the training data. The classifier performance was evaluated using the validation set. The trained model was then deployed to predict land cover across the study area.

2.3. Mapping Peatland Degradation

Peatland degradation is a critical environmental issue; remote sensing techniques are used on satellites. This study mapped peatland degradation using USGS Landsat 8 Level 2, Collection 2, Tier 1 from 2015 to 2023. We removed clouds and shadows from Landsat 8 imagery in GEE using the Quality Assessment (“QA_PIXEL”) band to mask out pixels with clouds and shadows. To create a cloud-free composite image, we used the median to combine multiple cloud-masked images into one representative image for a year.

We Applied an SMA algorithm to find the linear combination of endmember spectra that best matches the observed mixed pixel spectrum. The output of SMA is a set of fractional maps representing the spatial distribution of different land cover components within each pixel. These maps indicate the proportion of each endmember (e.g., vegetation, soil, water) present in each pixel. By comparing fractional maps from different periods, we

Table 2. Reflectance values of the Landsat-8 endmembers

| Endmember | Reflectance Values of Landsat-8 | | | | | |
|-----------|---------------------------------|-------------------|-----------------|-----------------|--------------------|--------------------|
| | Band 2 (Blue) | Band 3 (Green) | Band 4 (Red) | Band 5 (NIR) | Band 6 (SWIR 1) | Band 7 (SWIR 2) |
| NPV | 0.1514 | 0.1597 | 0.1421 | 0.3053 | 0.7707 | 0.1975 |
| GV | 0.0119 | 0.0475 | 0.0169 | 0.6250 | 0.2399 | 0.0675 |
| Soil | 0.1799 | 0.2479 | 0.3158 | 0.5437 | 0.7707 | 0.6646 |
| Cloud | 0.4031 | 0.8714 | 0.7900 | 0.8989 | 0.7002 | 0.6607 |

identified changes in the distribution of land cover components. It is beneficial for tracking the progression of peatland degradation, such as changes in vegetation and soil exposure.

We defined the Landsat-8 endmembers based on a previous study [Souza Jr. et al., 2005]. The pure reflectance values for the blue, green, red, NIR, SWIR1, and SWIR2 bands of the Landsat-8 for different endmember materials like NPV, GV, Soil, and Cloud are presented in Table 1.

Unmixing the Landsat-8 image using the built-in 'unmix()' function in Google Earth Engine involves estimating the fractional abundances of endmembers in each image pixel. The unmixed fractions were then converted to the image of the SMA model of the study area. The Shade and GVs fractions are used in the spectral mixture analysis to estimate the proportion of shaded and sunlit vegetation within a pixel. These fractions provide information about the vegetation canopy structure and can be calculated from the SMA results. The Shade fraction represents the pixel proportion covered by shadows or shaded areas. It is calculated by subtracting the sum of the GV and NPV fractions from 1:

$$\text{Shade} = 1 - (\text{GV} + \text{NPV}).$$

The GVs was accounted for the shading effect by dividing the Green Vegetation (GV) fraction by the complement of the Shade fraction:

$$\text{GV}_s = \frac{\text{GV}}{100 - \text{Shade}}.$$

The NDFI enhancing the degradation signal caused by selective logging and burning was computed using the derived fraction images by:

$$\text{NDFI} = \frac{\text{GV}_s - (\text{NPV} + \text{Soil})}{\text{GV}_s + \text{NPV} + \text{Soil}}.$$

Water and clouds affecting how we monitor forest degradation and loss were masked using a thresholding method based on the values of the fraction images. A water mask was created using threshold values for the Shade, GV, and Soil bands, where Shade is greater than or equal to 0.65, GV is less than or equal to 0.15, and Soil is less than or equal to 0.05. Meanwhile, a cloud mask was created by applying a threshold of 0.1 or more significant to the Cloud band.

Changes in NDFI that indicate forest change were obtained by calculating the difference between the two images. A temporal color composite was generated using two yearly NDFI images to enhance changes between them. The NDFI changes were then classified by defining a threshold based on inspecting the histogram and the NDFI temporal color composite.

3. Results and Discussion

3.1. Land cover analysis

Figure 2 shows the classified land cover over the study area. This land cover was classified into seven major land cover classes, i.e., tree cover, shrubland, grassland, cropland,

built-up, bare/sparse vegetation, and water bodies. The tree cover class includes peat forests, oil palm plantations, rubber plantations, and mangroves. We defined shrub class as woody perennial plants characterized by persistent, woody stems and no single, well-defined main stem, typically standing at a height of less than 5 meters. Any geographic area dominated by natural herbaceous plants (without persistent stems or shoots above ground and lacking defined hard structure) is classified as grass. Grasslands, prairies, steppes, savannahs, and pastures are examples of grasslands. Cropland refers to cultivated land that can be harvested at least once within a 12-month following the first sowing or planting. Built-up refers to areas occupied by buildings, roads, and various other human-made constructions, including railroads. Built-up refers to areas occupied by buildings, roads, and different other human-made constructions, including railroads. Furthermore, the term “water class” is employed to categorize various aquatic environments such as fish ponds, rivers, and other bodies of water.

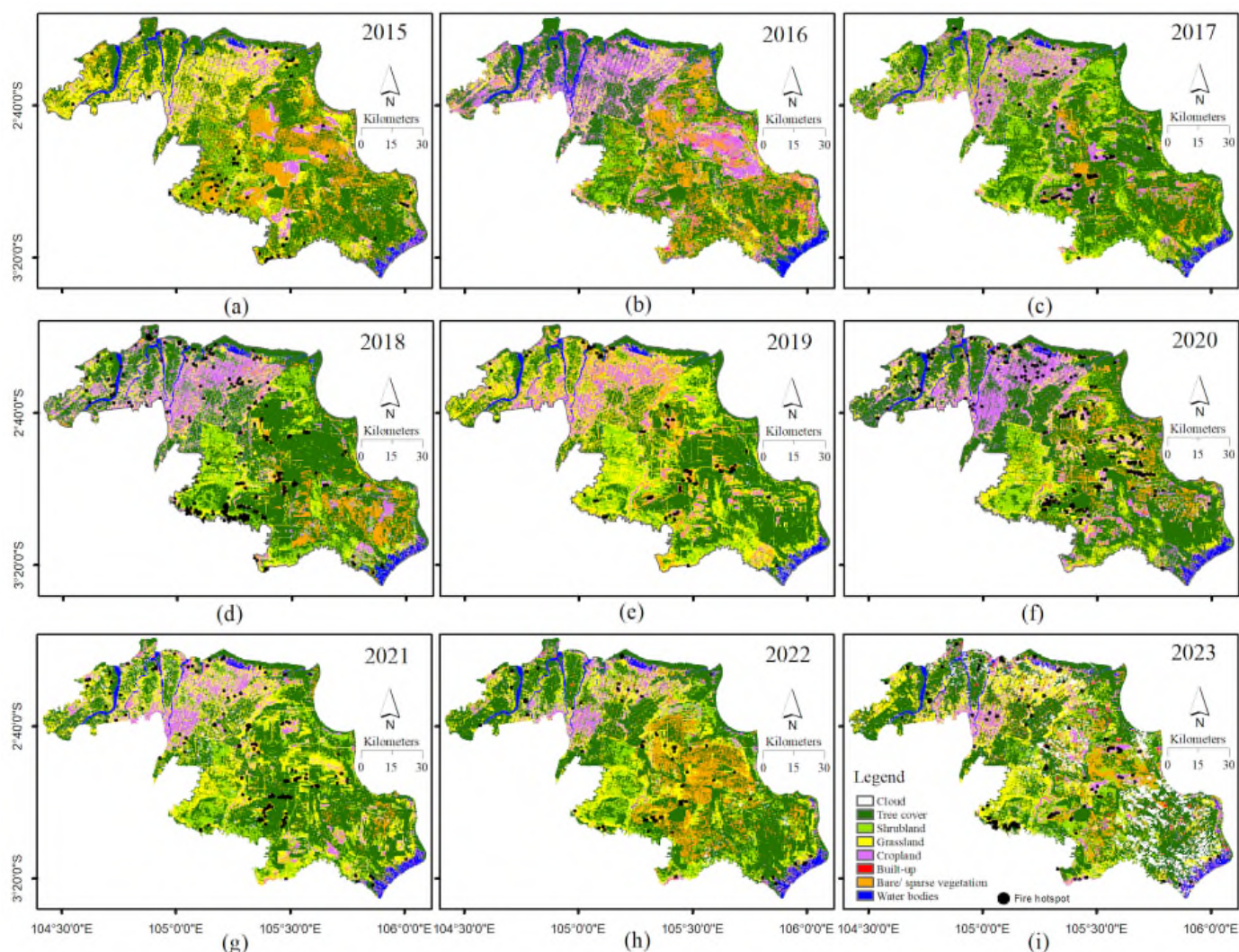


Figure 2. Classified land cover overlaid with hotspots from 2015–2023.

The overall accuracy (OA) of our land cover classification for 2015–2023 ranges from 90–94%, with a Kappa coefficient of 0.87–0.92, indicating a high level of accuracy and agreement between predicted and observed land cover classes, as shown in Table 3. The accuracy of the producers' (PA) and users' (UA) is also presented in this table. We randomly selected validation points to validate the classification and compared the predicted classes with observed land cover types in the field. The accuracy assessment showed that the model performed well across different land cover classes, with minimal misclassifications.

Table 3. Accuracy measurements of land cover

| Year | Kappa | OA | Tree Cover | | Shrubland | | Grassland | | Cropland | | Built-up | | Bare/sparse vegetation | | Water bodies | |
|------|-------|------|------------|------|-----------|------|-----------|------|----------|------|----------|------|------------------------|------|--------------|------|
| | | | PA | UA | PA | UA | PA | UA | PA | UA | PA | UA | PA | UA | PA | UA |
| 2015 | 0.92 | 0.94 | 0.96 | 1.00 | 1.00 | 0.90 | 0.85 | 0.86 | 0.80 | 0.80 | 0.67 | 1.00 | 1.00 | 0.94 | 1.00 | 1.00 |
| 2016 | 0.90 | 0.92 | 1.00 | 0.88 | 1.00 | 0.93 | 0.80 | 0.92 | 0.80 | 1.00 | 1.00 | 1.00 | 0.70 | 1.00 | 1.00 | 1.00 |
| 2017 | 0.87 | 0.90 | 0.94 | 0.91 | 0.82 | 0.90 | 0.90 | 0.90 | 0.80 | 1.00 | 1.00 | 1.00 | 1.00 | 0.80 | 0.71 | 1.00 |
| 2018 | 0.90 | 0.92 | 0.92 | 0.95 | 0.85 | 1.00 | 1.00 | 0.82 | 1.00 | 0.86 | 0.67 | 1.00 | 0.90 | 0.90 | 1.00 | 1.00 |
| 2019 | 0.88 | 0.91 | 1.00 | 0.97 | 0.86 | 0.86 | 0.94 | 0.76 | 0.57 | 1.00 | 0.00 | 0.00 | 0.81 | 1.00 | 1.00 | 1.00 |
| 2020 | 0.89 | 0.91 | 0.91 | 0.94 | 1.00 | 0.93 | 0.95 | 1.00 | 1.00 | 0.50 | 1.00 | 0.75 | 0.67 | 0.80 | 1.00 | 1.00 |
| 2021 | 0.90 | 0.93 | 1.00 | 0.89 | 1.00 | 0.90 | 1.00 | 1.00 | 1.00 | 1.00 | 1.00 | 1.00 | 0.62 | 1.00 | 1.00 | 1.00 |
| 2022 | 0.89 | 0.92 | 0.94 | 0.96 | 0.77 | 0.90 | 1.00 | 0.82 | 0.83 | 0.83 | 1.00 | 1.00 | 0.92 | 0.86 | 1.00 | 1.00 |
| 2023 | 0.87 | 0.90 | 0.96 | 1.00 | 0.67 | 1.00 | 0.91 | 0.83 | 0.80 | 0.67 | 0.67 | 1.00 | 1.00 | 0.75 | 1.00 | 1.00 |

Detailed information on the extent percentage of each class's area is presented in Figure 3. The tree cover shows some fluctuations over the years. Land cover changes in a region like South Sumatra can be complex and influenced by multiple factors spatially and temporally. The extreme climate, El Niño events, are generally associated with drier conditions and increased fire risk, leading to potential negative impacts on vegetation. Tree cover increased in 2017 and 2020 but was lower in 2015, 2019, and 2023, directly correlated with El Niño which had lower precipitation and drier over the study area. In such situations, vegetation may already be stressed and more susceptible to degradation.

By comparing our classification results with historical data, we observed a significant decrease in forest cover in 2019, indicated by low tree cover (47.1% of the total area of 1.054 million ha), primarily attributed to fires and logging. Therefore, grassland and bare/sparse vegetation had more significant coverage percentages, reaching 22.89% and 11.40%, respectively. It suggests that the severity of the peat fires in South Sumatra in 2019 might surpass those observed in 2015. However, both El Niño in 2015 and 2019 likely contributed to reduced precipitation in those years, which could have led to drier conditions and increased fire risk.

The increase in 2017 and 2020 could be related to recovery after the El Niño events. However, tree cover had a slightly larger percentage in 2015 than in 2016. The impact of an El Niño event on any specific vegetation type may not be immediate. It can take some time for the full effects of decreased precipitation and increased fire activity to manifest. In some ecosystems, fire is a natural and essential ecological process. Certain plant species have adaptations that allow them to thrive after a fire. However, intense fires can still lead to degradation if ecosystems cannot regenerate properly between fire events. In the case of the study area, the reduced precipitation and increased fire risk during the 2015 El Niño event might have directly affected shrubland in that year and tree cover in subsequent years, including 2016.

On the other hand, human activities play a significant role in shaping land cover changes. Human activities, such as agricultural burning, land clearing, or accidental ignition, start many fires. Most fires occurred over the cultivation area in the PHU of Sungai Saleh – Sungai Sugihan in 2015, 2018, and 2023. In these areas, drained peatlands were used for agriculture and cultivation. In areas where human-induced fires are common, vegetation degradation can occur due to the cumulative impact of these fires. On the other hand, many hotspots can also be identified in the protected area, especially in the PHU of Sungai Sugihan – Sungai Lumpur, in 2017, 2018, 2020, and 2021. Spatial correlations between land cover changes and fire hotspots often result from natural ecological processes, human activities, and environmental factors.

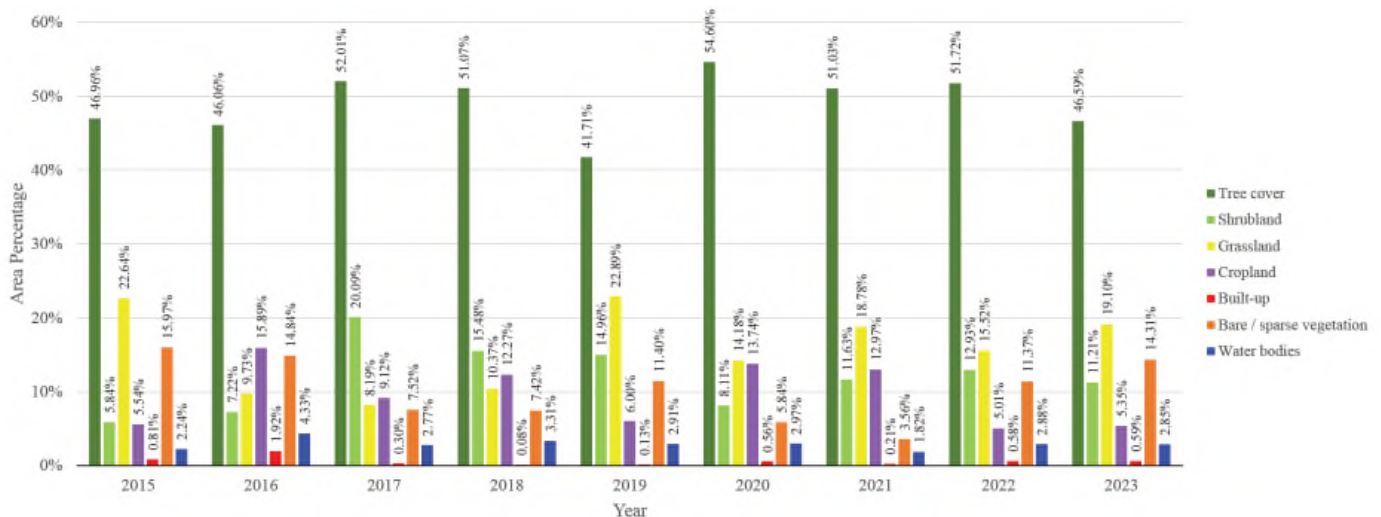


Figure 3. Percentages of classified land cover classes from 2015–2023.

3.2. Degradation analysis

This study also mapped peatland degradation to identify the factors causing changes in land cover. The data used for the degradation analysis consisted of Landsat-8 images from 2015 to 2023, covering the study area. The pure reflectance values for the blue, green, red, SWIR1, and SWIR2 spectral bands from the Landsat images were utilized for identifying endmembers such as NPV, GV, and Soil, as illustrated in Figure 4b–d. Unmixing the Landsat-8 images using the Singular Value Decomposition (SVD) method involved estimating the abundance fractions of endmembers in each image pixel.

The fractions obtained from the singular value decomposition were then transformed into a SMA model image for the study area. The Shade and GV fractions, as shown in Figure 4e,f, were used in spectral mixture analysis to estimate the proportions of vegetation in a pixel that was shaded and exposed to sunlight. These fractions provide information about the canopy structure of vegetation and can be computed from the SMA results. The Shade fraction represents the proportion of pixels covered by shadows or areas shaded by vegetation. Then, from the GV, NPV, and Soil fractions, the NDFI is calculated. For example, NDFI maps for 2019 and 2020 were used to map land degradation in 2020 by mapping the NDFI changes between these two consecutive years. The NDFI for those years and their changes can be displayed in Figure 4g–i.

Water and cloud, which can affect the mapping of forest degradation and damage, must be excluded from the calculations, often referred to as masking, using a threshold-based method based on the values of the fraction images. The water mask is created using threshold values for the Shade, GV, and Soil fractions, where Shade is greater than or equal to 0.65; GV is less than or equal to 0.15; and Soil is less than or equal to 0.05. Meanwhile, the cloud mask is created by applying a threshold of 0.1 or greater to the Cloud fraction.

Changes in NDFI indicating land changes are obtained by calculating the difference between these two images. A temporal color composite is generated using two annual NDFI images to highlight the changes between them. The changes in NDFI are then classified by defining thresholds and the temporal color composite of NDFI. In the Landsat 8 composite map (Figure 4a), green indicates vegetation, and brown represents bare land. Bare land without vegetation corresponds to what the Soil fraction map shows, which appears whiter. The whiter the color in the GV and GV's fraction maps, the more vegetated the area. Similarly, for other fraction maps, such as NPV and Shade, the whiter color indicates higher fraction values, reflecting the condition of the depicted objects.

Peatland degradation in South Sumatra, Indonesia, is primarily caused by human activity and environmental factors. Draining peatlands for agricultural purposes, particularly the creation of oil palm plantations and rice fields, upsets the natural hydrological

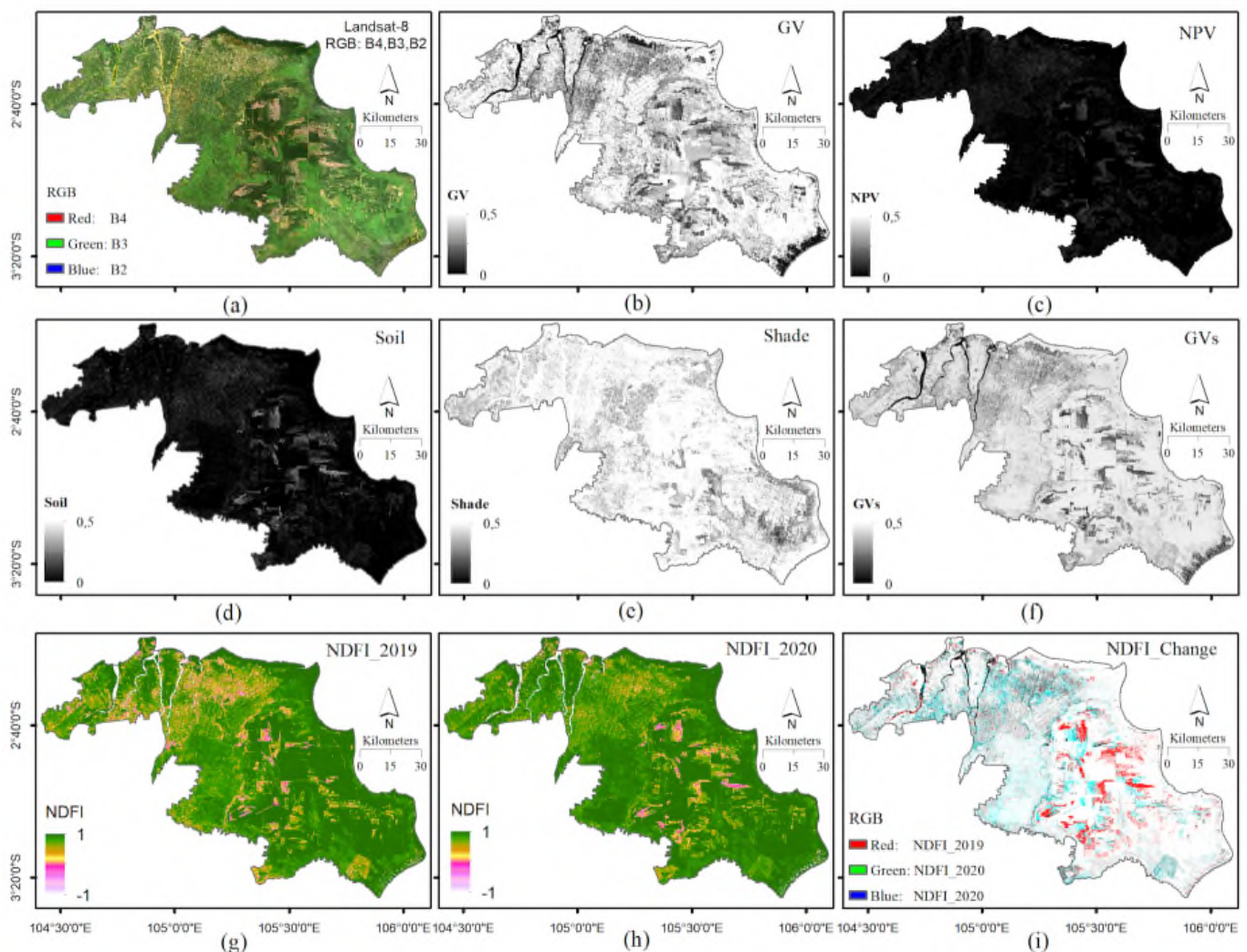


Figure 4. Maps of (a) Landsat-8 RGB composite, (b-f) Landsat-8 fractions, (g) NDFI 2019, (h) NDFI 2020, and (i) NDFI change from 2019–2020.

equilibrium, causing the water table to decrease and the peat to dry out. This accelerates the breakdown process and releases stored carbon into the environment. Large-scale land conversion exacerbates the problem, as enormous sections of peatland are removed and transformed into plantations. The loss of natural vegetation exposes the peat to oxidation, accelerating decomposition. Furthermore, the region is prone to peat fires, particularly during the dry season. Climate change exacerbates these difficulties by changing precipitation patterns and increasing the frequency of extreme weather events like droughts and wildfires, putting additional strain on already degraded peatlands. The orange on the NDFI maps (Figure 4g,h) indicates forest disturbance related to fires and selective logging. Meanwhile, the pink and white colors represent dry vegetation and bare land in previously logged forests. In grassland areas, the orange color indicates dry vegetation. The NDFI change map in Figure 4i used red to depict new deforestation, and pink represents selective logging. The cyan color indicates vegetation regrowth in areas logged or burned a year or more ago.

NDFI changes were classified to identify vegetation disturbances, deforestation, and vegetation regrowth spatially and temporally from 2015 to 2023, as presented in Figure 5. These maps are overlaid with the distribution of fire hotspots to analyze the relationship between the NDFI change classification and the locations of fire occurrences. Generally, these changes relatively corresponded to the identified hotspot distribution, indicating

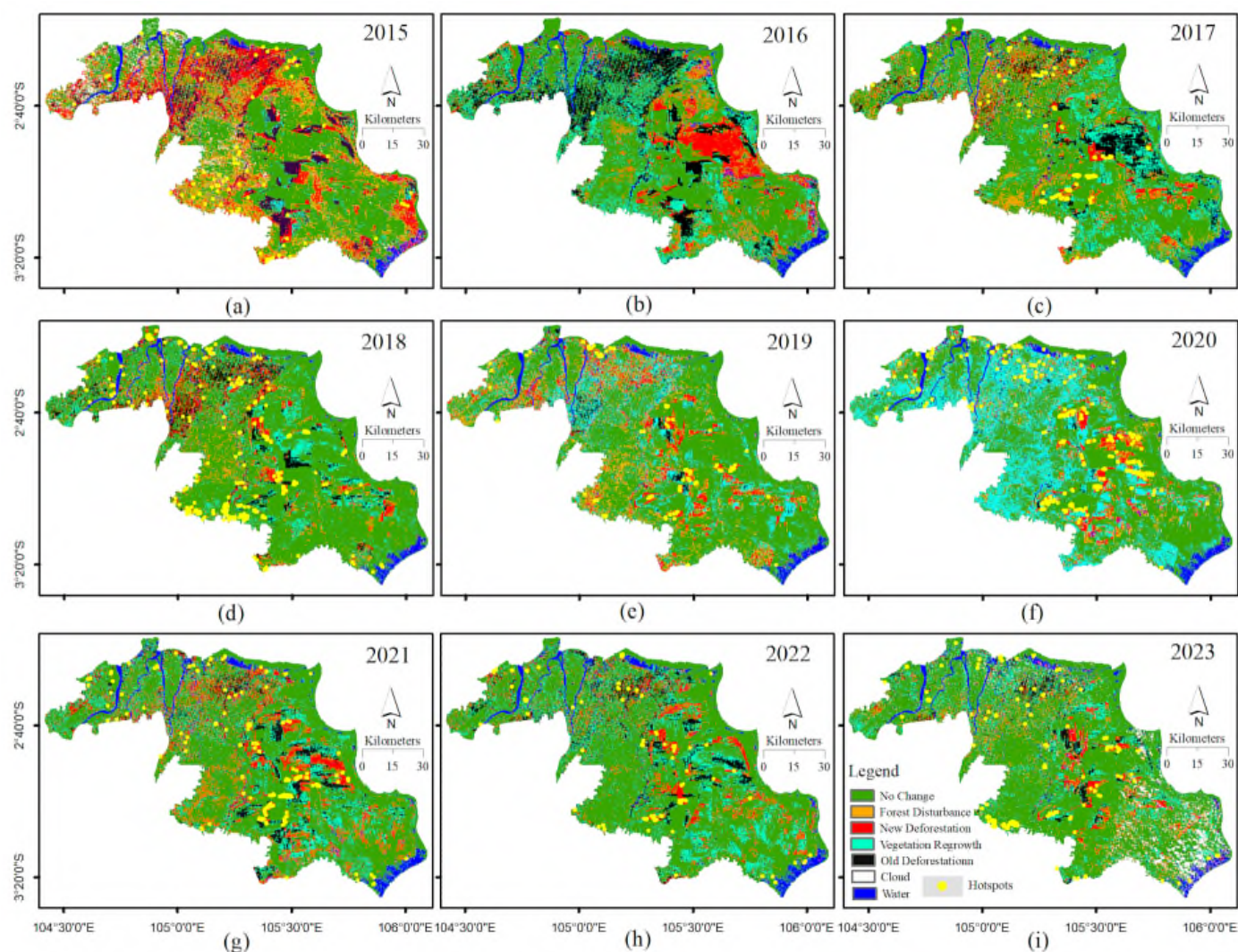


Figure 5. NDFI changes classes overlaid the hotspot from 2015–2023.

that the degradation caused by land fires obtained from the NDFI change classification aligns with the observed fire events. According to the NDFI change categorization map, the PHU of Sungai Sugihan – Sungai Lumpur, situated in the eastern region of the research area, had the highest degree of degradation. Subsequently, the adjacent PHU located to the west, specifically Sungai Saleh – Sungai Sugihan, exhibits a similarly significant level of degradation. Although these PHUs have encountered more severe degradation, it is essential to note that the peatland ecosystems within them exhibit distinct characteristics. Specifically, the PHU Sungai Saleh – Sungai Sugihan encompasses cultivated areas, whereas the PHU Sungai Sugihan – Sungai Lumpur comprises protected areas.

In addition, the extent of the percentage of degraded areas can be calculated based on the NDFI change classification, as presented in Figure 6. According to these calculations, the most severe degradation occurred in 2015, followed by 2019. The percentage of no forest change has gradually increased from 2015 to 2018, showing that these areas have comparatively recovered from the effects of the El Niño in 2015. On the other hand, it declined between 2019 and 2020 before climbing back up to 2023. Forest disturbance includes activities that negatively impact the forest but may not necessarily result in deforestation. This category covers disturbances such as logging, selective harvesting, or fires. Forest disturbance decreased from 2015 to 2018 but slightly increased in the last few years. New deforestation refers to converting forested areas into non-forest land cover

types. It indicates the loss of forested land. New deforestation varied over the years but showed a declining trend from 2015 to 2023, suggesting that efforts might have been made to reduce deforestation. Vegetation regrowth represents areas where new vegetation has grown, naturally or through reforestation, following previous disturbances. Vegetation regrowth increased notably from 2016 to 2020 and remained relatively stable afterward. It may indicate successful reforestation or natural regeneration.

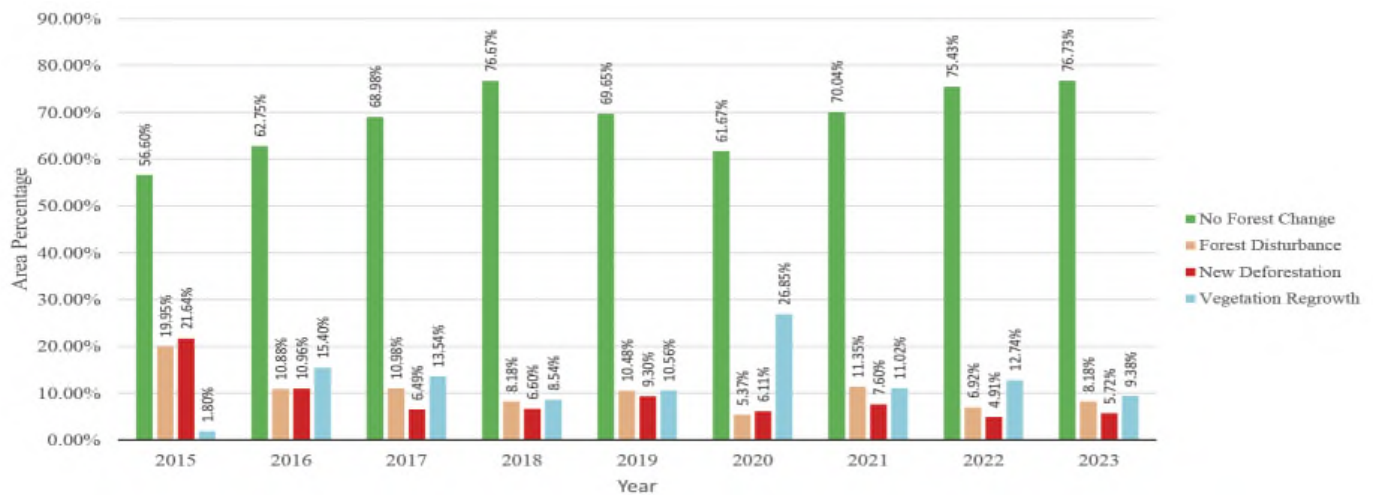


Figure 6. Variation of area percentages for four NDFI change classes from 2015–2023.

Key observations from the results are the data suggests that there has been a reduction in new deforestation over the years, which is a positive sign for forest conservation efforts; the increase in vegetation regrowth from 2016 to 2020 is noteworthy and indicates restoration efforts or natural recovery in previously disturbed areas; forest disturbance decreased from 2015 to 2020 but showed a slight increase in the last few years, which should be monitored to ensure sustainable forest management practices.

4. Conclusion

Our study analyzed land cover dynamics and forest degradation in South Sumatra's peatlands from 2015 to 2023 using Random Forest classification and NDFI change analysis with a multi-temporal dataset from Sentinel-1, Sentinel-2, and Landsat-8. The classification results showed seven land cover classes consisting of tree cover, shrubland, grassland, farmland, built-up regions, bare/sparse vegetation, and water bodies, offering a comprehensive picture of land cover changes in the study area. Accuracy of 90% to 94% and a Kappa coefficient of 0.87 to 0.92 shows significant agreement between predicted and actual land cover classifications across categories. Our classification model's low misclassification rate proves its usefulness for monitoring peatland land cover changes.

The comprehensive examination of land cover alterations throughout the study unveiled variations in the extent of tree cover, which were impacted by intricate spatial and temporal factors. It is worth mentioning that the effects of El Niño occurrences, which are linked to arid conditions and heightened susceptibility to fires, were noted during periods of diminished tree coverage. The year 2019 experienced a notable decline in forest area, predominantly because of fires and logging operations. Consequently, there was an expansion in grassland coverage and an increase in areas with limited or no vegetation. Forest disturbance increased slightly in recent years after decreasing from 2015 to 2020. Anthropogenic activities, such as the deliberate burning of agricultural fields and the clearance of land, have significantly influenced alterations in land cover. The areas in the two PHUs have more severe degradation, and the gradation occurred in regions with distinct peatland ecosystem functions. The PHU of Sungai Saleh – Sungai Sugihan degraded mainly in the cultivation area, while the PHU of Sungai Sugihan – Sungai Lumpur in the protected areas.

The areas with the highest levels of fire activity were primarily located in regions where fires caused by human activities were prevalent, namely on drained peatlands utilized for agricultural purposes. Furthermore, the presence of fire hotspots was seen within designated protected areas, indicating the intricate relationship between natural biological processes, human actions, and environmental elements in influencing alterations in land cover and degradation of forests.

Our study suggests that South Sumatra peatlands are ecologically important and vulnerable to natural and human-induced processes, making monitoring and conservation essential. Advanced remote sensing and historical data help policymakers and land managers establish proactive policies to conserve these vital ecosystems in the face of changing environmental challenges.

Acknowledgments. We would like to acknowledge Direktorat Riset, Teknologi, dan Pengabdian kepada Masyarakat (DRTPM) for financial support through “Penelitian Fundamental Regular”, Contract Number: 164/E5/PG.02.00.PL/2023, dated 5 July 2023. We also thank the European Space Agency (ESA) for providing Sentinel-1 data, anonymous reviewers, and the academic editor for their valuable comments and suggestions.

References

- Adams, J. (1995), Classification of multispectral images based on fractions of endmembers: Application to land-cover change in the Brazilian Amazon, *Remote Sensing of Environment*, 52(2), 137–154, [https://doi.org/10.1016/0034-4257\(94\)00098-8](https://doi.org/10.1016/0034-4257(94)00098-8).
- Amoakoh, A. O., P. Aplin, K. T. Awuah, et al. (2021), Testing the Contribution of Multi-Source Remote Sensing Features for Random Forest Classification of the Greater Amanzule Tropical Peatland, *Sensors*, 21(10), 3399, <https://doi.org/10.3390/s21103399>.
- Asmuß, T., M. Bechtold, and B. Tiemeyer (2019), On the Potential of Sentinel-1 for High Resolution Monitoring of Water Table Dynamics in Grasslands on Organic Soils, *Remote Sensing*, 11(14), 1659, <https://doi.org/10.3390/rs11141659>.
- Astuti, R. (2021), Governing the ungovernable: The politics of disciplining pulpwood and palm oil plantations in Indonesia’s tropical peatland, *Geoforum*, 124, 381–391, <https://doi.org/10.1016/j.geoforum.2021.03.004>.
- Breiman, L. (2001), Random Forests, *Machine Learning*, 45(1), 5–32, <https://doi.org/10.1023/A:1010933404324>.
- Budiman, I., R. D. Hapsari, C. I. Wijaya, and E. N. N. Sari (2021), The Governance of Risk Management on Peatland: A Case Study of Restoration in South Sumatra, Indonesia, *World Resources Institute*, <https://doi.org/10.46830/wriwp.20.00008>.
- Carrasco, L., A. W. O’Neil, R. D. Morton, and C. S. Rowland (2019), Evaluating Combinations of Temporally Aggregated Sentinel-1, Sentinel-2 and Landsat 8 for Land Cover Mapping with Google Earth Engine, *Remote Sensing*, 11(3), 288, <https://doi.org/10.3390/rs11030288>.
- Chokkalingam, U., Suyanto, R. P. Permana, et al. (2006), Community fire use, resource change, and livelihood impacts: The downward spiral in the wetlands of southern Sumatra, *Mitigation and Adaptation Strategies for Global Change*, 12(1), 75–100, <https://doi.org/10.1007/s11027-006-9038-5>.
- Cobb, A. R., A. M. Hoyt, L. Gandois, et al. (2017), How temporal patterns in rainfall determine the geomorphology and carbon fluxes of tropical peatlands, *Proceedings of the National Academy of Sciences*, 114(26), <https://doi.org/10.1073/pnas.1701090114>.
- Cooper, H. V., S. Evers, P. Aplin, N. Crout, M. P. B. Dahalan, and S. Sjogersten (2020), Greenhouse gas emissions resulting from conversion of peat swamp forest to oil palm plantation, *Nature Communications*, 11(1), <https://doi.org/10.1038/s41467-020-14298-w>.
- Dohong, A. (2017), Bolstering Peatlands Restoration in Indonesia through 3Rs Approach, in *Developing International Collaborations to Address Fire and Other Conservation Issues in Central Kalimantan, Indonesia*, <https://doi.org/10.13140/RG.2.2.33080.19200>.

- Dohong, A., A. A. Aziz, and P. Dargusch (2017), A review of the drivers of tropical peatland degradation in South-East Asia, *Land Use Policy*, 69, 349–360, <https://doi.org/10.1016/j.landusepol.2017.09.035>.
- Dommain, R., J. Couwenberg, P. H. Glaser, et al. (2014), Carbon storage and release in Indonesian peatlands since the last deglaciation, *Quaternary Science Reviews*, 97, 1–32, <https://doi.org/10.1016/j.quascirev.2014.05.002>.
- Filgueiras, R., E. C. Mantovani, D. Althoff, E. I. Fernandes Filho, and F. F. da Cunha (2019), Crop NDVI Monitoring Based on Sentinel 1, *Remote Sensing*, 11(12), 1441, <https://doi.org/10.3390/rs11121441>.
- Gómez, C., J. C. White, and M. A. Wulder (2016), Optical remotely sensed time series data for land cover classification: A review, *ISPRS Journal of Photogrammetry and Remote Sensing*, 116, 55–72, <https://doi.org/10.1016/j.isprsjprs.2016.03.008>.
- Harrison, M. E., J. B. Ottay, L. J. D’Arcy, et al. (2019), Tropical forest and peatland conservation in Indonesia: Challenges and directions, *People and Nature*, 2(1), 4–28, <https://doi.org/10.1002/pan3.10060>.
- Hidayah, H., J. Reidinar, N. S. Tjokorda, and W. Arief (2018), Indonesia’s Deforestation Dropped 60 Percent in 2017, but There’s More to Do, <https://www.wri.org/insights/indonesias-deforestation-dropped-60-percent-2017-theres-more-do>.
- Hooijer, A., S. Page, J. G. Canadell, M. Silvius, J. Kwadijk, H. Wösten, and J. Jauhiainen (2010), Current and future CO₂ emissions from drained peatlands in Southeast Asia, *Biogeosciences*, 7(5), 1505–1514, <https://doi.org/10.5194/bg-7-1505-2010>.
- Humas (2016), President Jokowi Establishes Peat Land Restoration Agency (BRG), <https://setkab.go.id/en/president-jokowi-establishes-peat-land-restoration-agency-brg/>.
- Khakim, M. Y. N., A. A. Bama, I. Yustian, P. Poerwono, T. Tsuji, and T. Matsuoka (2020), Peatland subsidence and vegetation cover degradation as impacts of the 2015 El niño event revealed by Sentinel-1A SAR data, *International Journal of Applied Earth Observation and Geoinformation*, 84, 101,953, <https://doi.org/10.1016/j.jag.2019.101953>.
- Khakim, M. Y. N., A. A. Bama, and T. Tsuji (2022), Spatiotemporal Variations of Soil Moisture and Groundwater Level in a South Sumatra Peatland, Indonesia During 2015-2018, *GEOGRAPHY, ENVIRONMENT, SUSTAINABILITY*, 15(2), 58–70, <https://doi.org/10.24057/2071-9388-2021-137>.
- KLHK (2020), Karhutla Monitoring System, <https://sipongi.menlhk.go.id/>.
- Malinowski, R., S. Lewiński, M. Rybicki, et al. (2020), Automated Production of a Land Cover/Use Map of Europe Based on Sentinel-2 Imagery, *Remote Sensing*, 12(21), 3523, <https://doi.org/10.3390/rs12213523>.
- Miettinen, J., A. Hooijer, C. Shi, et al. (2012), Extent of industrial plantations on Southeast Asian peatlands in 2010 with analysis of historical expansion and future projections, *GCB Bioenergy*, 4(6), 908–918, <https://doi.org/10.1111/j.1757-1707.2012.01172.x>.
- Miettinen, J., A. Hooijer, R. Vernimmen, S. C. Liew, and S. E. Page (2017), From carbon sink to carbon source: extensive peat oxidation in insular Southeast Asia since 1990, *Environmental Research Letters*, 12(2), 024,014, <https://doi.org/10.1088/1748-9326/aa5b6f>.
- Numata, I., A. J. Elmore, M. A. Cochrane, C. Wang, J. Zhao, and X. Zhang (2022), Deforestation, plantation-related land cover dynamics and oil palm age-structure change during 1990-2020 in Riau Province, Indonesia, *Environmental Research Letters*, 17(9), 094,024, <https://doi.org/10.1088/1748-9326/ac8a61>.
- Nurhayati, A. D., B. Hero Saharjo, L. Sundawati, S. Syartinilia, and M. A. Cochrane (2021), Forest and Peatland Fire Dynamics in South Sumatra Province, *Forest and Society*, pp. 591–603, <https://doi.org/10.24259/fs.v5i2.14435>.
- Page, S. E., J. O. Rieley, and C. J. Banks (2011), Global and regional importance of the tropical peatland carbon pool, *Global Change Biology*, 17(2), 798–818, <https://doi.org/10.1111/j.1365-2486.2010.02279.x>.
- Pettorelli, N., K. Safi, and W. Turner (2014), Satellite remote sensing, biodiversity research and conservation of the future, *Philosophical Transactions of the Royal Society B: Biological Sciences*, 369(1643), 20130,190, <https://doi.org/10.1098/rstb.2013.0190>.

- Poortinga, A., K. Tenneson, A. Shapiro, et al. (2019), Mapping Plantations in Myanmar by Fusing Landsat-8, Sentinel-2 and Sentinel-1 Data along with Systematic Error Quantification, *Remote Sensing*, 11(7), 831, <https://doi.org/10.3390/rs11070831>.
- Putra, R., E. Sutriyo, S. Kadir, and I. Iskandar (2019), Understanding of Fire Distribution in the South Sumatra Peat Area During the Last Two Decades, *International Journal of GEOMATE*, 16(54), <https://doi.org/10.21660/2019.54.8243>.
- Sakti, A. D., and S. Tsuyuki (2015), Spectral Mixture Analysis (SMA) of Landsat Imagery for Land Cover Change Study of Highly Degraded Peatland in Indonesia, *The International Archives of the Photogrammetry, Remote Sensing and Spatial Information Sciences*, XL-7/W3, 495–501, <https://doi.org/10.5194/isprsarchives-XL-7-W3-495-2015>.
- Schultz, M., J. G. P. W. Clevers, S. Carter, et al. (2016), Performance of vegetation indices from Landsat time series in deforestation monitoring, *International Journal of Applied Earth Observation and Geoinformation*, 52, 318–327, <https://doi.org/10.1016/j.jag.2016.06.020>.
- Shih, H., D. A. Stow, K. Chang, D. A. Roberts, and K. G. Goulias (2021), From land cover to land use: applying random forest classifier to Landsat imagery for urban land-use change mapping, *Geocarto International*, 37(19), 5523–5546, <https://doi.org/10.1080/10106049.2021.1923827>.
- Souza Jr., C. M., D. A. Roberts, and M. A. Cochrane (2005), Combining spectral and spatial information to map canopy damage from selective logging and forest fires, *Remote Sensing of Environment*, 98(2-3), 329–343, <https://doi.org/10.1016/j.rse.2005.07.013>.
- Souza Jr., C. M., J. V. Siqueira, M. H. Sales, et al. (2013), Ten-Year Landsat Classification of Deforestation and Forest Degradation in the Brazilian Amazon, *Remote Sensing*, (5), 5493–5513, <https://doi.org/10.3390/rs5115493>.
- Tian, S., X. Zhang, J. Tian, and Q. Sun (2016), Random Forest Classification of Wetland Landcovers from Multi-Sensor Data in the Arid Region of Xinjiang, China, *Remote Sensing*, 8(11), 954, <https://doi.org/10.3390/rs8110954>.
- Toca, L., R. R. E. Artz, C. Smart, et al. (2023), Potential for Peatland Water Table Depth Monitoring Using Sentinel-1 SAR Backscatter: Case Study of Forsinard Flows, Scotland, UK, *Remote Sensing*, 15(7), 1900, <https://doi.org/10.3390/rs15071900>.
- Uda, S. K., G. Schouten, and L. Hein (2020), The institutional fit of peatland governance in Indonesia, *Land Use Policy*, 99, 103,300, <https://doi.org/10.1016/j.landusepol.2018.03.031>.
- Urban, M., C. Berger, T. E. Mudau, et al. (2018), Surface Moisture and Vegetation Cover Analysis for Drought Monitoring in the Southern Kruger National Park Using Sentinel-1, Sentinel-2, and Landsat-8, *Remote Sensing*, 10(9), 1482, <https://doi.org/10.3390/rs10091482>.
- Vijay, V., S. L. Pimm, C. N. Jenkins, and S. J. Smith (2016), The Impacts of Oil Palm on Recent Deforestation and Biodiversity Loss, *PLOS ONE*, 11(7), e0159,668, <https://doi.org/10.1371/journal.pone.0159668>.
- Yamada, Y. (2015), Preliminary Study on the Radar Vegetation Index (RVI) Application to Actual Paddy Fields by ALOS/PALSAR Full-polarimetry SAR Data, *The International Archives of the Photogrammetry, Remote Sensing and Spatial Information Sciences*, XL-7/W3, 129–131, <https://doi.org/10.5194/isprsarchives-XL-7-W3-129-2015>.
- Yuwati, T. W., D. Rachmanadi, Pratiwi, M. Turjaman, et al. (2021), Restoration of Degraded Tropical Peatland in Indonesia: A Review, *Land*, 10(11), 1170, <https://doi.org/10.3390/land10111170>.
- Zheng, X., C. Wang, Y. Tang, et al. (2023), Adaptive High Coherence Temporal Subsets SBAS-InSAR in Tropical Peatlands Degradation Monitoring, *Remote Sensing*, 15(18), 4461, <https://doi.org/10.3390/rs15184461>.